Comparison of different constitutive models to characterize the viscoelastic properties of human abdominal adipose tissue. A pilot study.

Jose L Calvo-Gallego[a,d,*], Jaime Domínguez[a], Tomás Gómez Cía[b], Gorka Gómez Ciriza[c], Javier Martínez-Reina[a]

[a] *Department of Mechanical Engineering, University of Seville, Camino de los Descubrimientos s/n, Seville 41092, Spain*
[b] *Cirugía Plástica y Grandes Quemados, Hospital Virgen del Rocío, Seville, Spain*
[c] *Grupo de Innovación Tecnológica, Hospital Virgen del Rocío, Seville, Spain*
[d] *Fundación Ayesa, Avd. Marie Curie 2, PCT Cartuja, Seville 41092, Spain*

Abstract

Knowing the mechanical properties of human adipose tissue is key to simulate surgeries such as liposuction, mammoplasty and many plastic surgeries in which the subcutaneous fat is present. One of the most important surgeries, for its incidence, is the breast reconstruction surgery that follows a mastectomy. In this case, achieving a deformed shape similar to the healthy breast is crucial. The reconstruction is most commonly made using autologous tissue, taken from the patient's abdomen. The amount of autologous tissue and its mechanical properties have a strong influence on the shape of the reconstructed breast. In this work, the viscoelastic mechanical properties of the human adipose tissue have been studied. Uniaxial compression stress relaxation tests were performed in adipose tissue specimens extracted from the human abdomen. Two different viscoelastic models were used to fit to the experimental tests: a quasi-linear viscoelastic (QLV) model and an internal variables viscoelastic (IVV) model; each one with four different hyperelastic strain energy density functions to characterise the elastic response: a 5-terms polynomial function, a first order Ogden function, an isotropic Gasser-Ogden-Holzapfel function and a combination of a neo-Hookean and an exponential function. The IVV model with the Ogden function was the best combination to fit the experimental tests. The viscoelastic properties are not important in the simulation of the static deformed shape of the breast, but they are needed in a relaxation test performed under finite strain rate, particularly, to derive the long-term behaviour (as time tends to infinity), needed to estimate the static deformed shape of the breast. The so obtained stiffness was compared with previous results given in the literature for adipose tissue of different regions, which exhibited a wide dispersion.

Keywords:

human adipose tissue, abdomen, stress relaxation test, viscoelasticity, mechanical properties

[*] Corresponding author. Tel.: +34-954487311; fax: +34-954460475.
Email address: joselucalvo@us.es (Jose L Calvo-Gallego)

1. Introduction

The adipose tissue is involved in many surgeries. For instance, in plastic surgery, in which fat is always present as subcutaneous adipose tissue or in liposuction, in which the aim is to eliminate it. In other cases, the adipose tissue is removed from one anatomical site to be implanted in a different one. This is the case of breast reconstruction with autologous tissue, such as for example the deep inferior epigastric artery perforator flap surgery (DIEAP). In this surgery, after a mastectomy is performed in the women breast due to cancer, the breast is reconstructed using tissue from the patient's abdomen. The advantage of this technique against prosthetic breast reconstruction is that the risk of rejection is minimized. Although DIEAP surgery is more expensive and needs a longer surgical time than breast tissue expander and prostheses surgeries, recent studies have showed that the former is cost-effective in comparison to the latter [33, 36]. One aim of the reconstruction is mimicking the deformed shape of the healthy breast and that is influenced by the amount of implanted tissue and its mechanical properties. Therefore, the assessment of these properties is key in Finite Element (FE) simulations of the surgery, which may help in pre-operative planning.

Many examples of these FE simulations can be found in the literature: to predict the location of a tumour [2, 43]; to simulate the compression of the breast between two plates, like in a mammography [2, 24, 41, 43, 49]; for image registration, normally performing also a compression [23, 28–30, 38, 46, 47, 52]; to simulate the deformed shape under gravity loads in standing position [18, 21, 42, 44, 45, 60]; to simulate a prosthesis insertion for augmentation mammoplasty [35], etc. Moreover, some FE models addressing the mechanical properties of the fat of other anatomical sites, like the calcaneal fat pad [37, 40], can be found in the literature. Probably, the main limitation of these studies is the lack of a solid knowledge of the mechanical properties of the adipose tissue.

The adipose tissue is a loose connective tissue in which adipocytes are the main cellular component. Adipocytes are separated and supported by connective tissue septa. The adipose tissue plays a fundamental role in energy homeostasis, but it also has a structural function, serving as a padding to protect other organs.

Most authors have considered the adipose tissue as isotropic, in computational simulations [2, 18, 23, 28–30, 35, 41–47, 49, 52, 60] as well as fitting experimental tests [9–11, 39, 48, 50, 51, 53, 55, 57]. Recently, Sommer et al. [56] considered it as an anisotropic material with one family of fibres, by identifying a preferential direction in the connective tissue that surrounds the adipocytes. However, those authors gave no reason to consider only one family of fibres. Furthermore, they did not determine the fibre direction through histological studies, but in a phenomenological way. Therefore, it is difficult to use this fibred model in a FE simulation. All the previously cited works considered adipose tissue as an incompressible material. Finally, there are some studies in which the viscoelastic behaviour of the adipose tissue has been clearly identified and described [56].

As stated above, there is not much information in the literature about the mechanical properties of the adipose tis-

sue, let alone for the human adipose tissue. The most studied animal tissue has been porcine subdermal fat. Geerligs et al. [20] performed shear tests on this tissue with a special focus on its viscoelastic behaviour. In the linear viscoelastic regime, they analysed the storage and loss modulus and its dependency on temperature and frequency. They also introduced a power law function to describe the frequency dependent behaviour and the stress relaxation behaviour. Comley and Fleck [10, 11] performed shear and uniaxial compression tests in a wide range of strain rates. They fitted a first order Ogden model to the experimental results. These authors also studied the toughness of this tissue [12]. Sims et al. [55] performed indentation tests, fitting a neo-Hookean model with Prony series to model the time dependent behaviour. Few authors have studied human adipose tissue. Bennett and Ker [3] carried out indentation tests on the heel pad from amputated limbs, showing the force-displacement relation but not providing any model to fit the experimental results. Miller-Young et al. [39] performed quasi-static and relaxation compression tests on human cadaveric heel pads. They fitted the results using a Mooney-Rivlin model and an exponential decay to account for the change in the material constants over time. Samani et al. performed indentation tests on human breast fat, modelling it as a linear elastic material [48, 51] and as a hyperelastic material, modelled with a 5-terms polynomial strain energy density (SED) function [50]. Chen and Weiland [9] carried out uniaxial tension tests on the orbital fat of pigs and humans. They fitted the results with a linear elastic model. Then et al. [57] performed *in vivo* cyclic indentation and relaxation tests in human gluteal tissue. They used a computational simulation to fit a quasi-linear viscoelastic (QLV) model to the skin and fat (considered as a unique material) and the muscle (only the passive state). Sommer et al. [56] carried out biaxial and shear tests on human abdominal adipose tissue and fitted the results using the Gasser-Ogden-Holzapfel (GOH) hyperelastic model with one family of fibres.

As can be seen in those works, there are not many studies about human adipose tissue. Most of them were carried out on the heel pad and only one in the abdominal fat, which is key for the breast reconstruction. Concerning the viscoelastic properties, although some authors has highlighted the viscous behaviour of the adipose tissue, few works have studied such properties. Therefore, there is little knowledge about the viscoelastic properties of human adipose tissue, despite their importance in breast reconstruction.

The global objective of the project this study belongs to is to characterize the viscoelastic behaviour of the human adipose tissue. The present work is a pilot study in which a model is proposed to simulate that behaviour: using two different viscoelastic models and several SED functions for the elastic part of the response, in order to choose the most adequate combination of models (visco and elastic). To the author's knowledge, this is the first work that investigates the viscoelastic properties of the human abdominal adipose tissue. These properties will aid to improve the FE simulations of process in which this tissue is involved, for example, breast reconstruction with autologous tissue.

2. Materials and methods

2.1. Test protocol

2.1.1. Preparation of specimens

The adipose tissue samples were extracted from the abdomen of a 57 years old female patient subjected to a DIEAP surgery. Specifically, they were extracted from a piece of adipose tissue removed from the abdomen (see figure 1), but not eventually needed for the reconstruction.

The pieces were transported from the hospital to the laboratory in a cool-box with dry ice right after the surgery. In less than 30 minutes the pieces were in the laboratory where the skin and the most superficial fat layer were removed by cutting a slice of tissue (or flap) of approximately 5 mm in depth (see figure 1), ensuring that the piece had approximately parallel faces. Depending on the thickness of the extracted abdominal flap, the height of the tested specimens ranged from 5 to 10 mm, which is equal or lower than that used by Miller-Young et al. [39], and was limited to that range to prevent specimens from buckling during the compression tests. The adipose tissue is very soft at room temperature and, consequently, it was difficult to obtain a slice of parallel faces by cutting it at that temperature. Thus, the slice was cut while the tissue was thawing.

The reconstruction surgery is quite long and, consequently, the mechanical test could not be performed on the same day of extraction. Thus, the slice was frozen to avoid degradation of the tissue. It was wrapped in saline-soaked gauze (saline solution: 0.9% w/v of NaCl); wrapped in a plastic film and introduced in hermetic vials to prevent dehydration; and finally frozen at -20°C until the following day, when the tests were carried out.

The mechanical tests were performed in cylindrical specimens, extracted from the slice by slowly pushing a hollow punch of 19 mm in diameter against the slice. This extraction had to be done while the slice was frozen. Otherwise, the final shape of the specimens was irregular and far from cylindrical, because the tissue was largely deformed by the punch. A specimen with the final cylindrical shape can be seen in figure 2. Next, the specimen was submerged in saline solution at room temperature and allowed to thaw. Then, it was digitally photographed to measure its cross-sectional area through computerised image analysis. Placing *ex-vivo* adipose tissue specimens under physiological temperature often leads to a significant change in specimen geometry, which may render the measurement very difficult and inaccurate. Nonetheless, this was not the case in this study due to the small size of the specimens.

2.1.2. Relaxation test

The specimens were subjected to a relaxation test under unconfined uniaxial compression between two platens. A servo-hydraulic testing machine (858 Mini Bionix II, MTS, Eden Prairie, USA) was used to apply the compression.

To ensure that the test was performed under physiologic conditions of humidity and temperature, the experimental setup, shown in figure 3, included a methacrylate recipient filled with saline solution, that was kept at 37 ± 1 °C by means of a heater and thermostat. This experimental setup was already used in a previous study in which the same test was performed on temporomandibular articular discs [13].

The following procedure was followed to perform the tests. First, both platens of the testing machine were brought into contact with the specimen's top and bottom surface and at this point the displacement was zeroed. Then, the upper platen was moved upward and some vaseline was spread on the surface of both platens to reduce friction and facilitate the sliding of the specimens. Once the specimen was thawed, it was placed at the center of the inferior platen of the testing machine. Unlike the previous work referred to above [13], here the specimen was not glued to the inferior platen to prevent it from slipping off. In this case, gluing was not necessary to keep the specimens between the platens and, besides, this allowed to get a stress state closer to uniaxial [14]. Next, the upper platen was moved downwards, slowly approaching the sample, and visually positioned in contact with the top surface of the sample, as made in [39]. That allowed to measure the thickness of the specimen and to define the starting point of the test.

A preconditioning load was applied to each sample consisting in 20 cycles from 0% to 10% strain at 1 Hz, like in [1]. This was followed by a ramp from 0% to 50% strain, like in [13, 39]. This final strain was maintained for 15 minutes, allowing for stress relaxation (see figure 4). The strain level used here corresponds to the breast compression reported by some authors [24, 47]. Different strain rates were applied for the loading ramp: 50%, 60% and $70\%/s$. The strain rate was limited to that range for practical reasons. The stresses were extremely sensitive to the strain rate and particularly outside that range. To be precise, the specimens were severely damaged using faster rates, while the resulting stresses were very small for slower rates. In order to keep a low measurement uncertainty for those slower rates, a different procedure or equipment should have been used, but then the measurement uncertainty would have appeared for the higher strain rates. So, to be able to measure the stresses using a single procedure/equipment, the strain rates were limited to the range referred to above, which in turn was the range used by other authors [39].

The applied force, $F(t)$, and the displacement of the upper platen $u(t)$ were continuously recorded during the test. The lower platen was fixed. From these data, the experimental Cauchy stress, $\overline{\sigma}$, was estimated assuming uniaxial compression and incompressibility, through:

$$\overline{\sigma}(t) = \frac{F(t)\,\lambda(t)}{A_0} \tag{1}$$

where A_0 is the initial cross-sectional area of the sample and $\lambda(t)$ is the principal stretch in the loading direction, given by:

$$\lambda(t) = 1 + \frac{u(t)}{L_0} \tag{2}$$

being L_0 the initial length of the specimen. In the case of compression $u(t) < 0$ and $\lambda(t) < 1$.The experimental stress record was fitted using two different viscoelastic models described hereunder.

2.2. Data fitting algorithm: quasi-linear viscoelastic model

The quasi-linear viscoelastic (QLV) model has been widely used to model the behaviour of soft tissues [7, 13, 16, 17, 59]. For a general stretch history, $\lambda = \lambda(t)$, the temporal evolution of stress is given by equation (3). Here, the stretch history is given in figure 4, but it must be noted that the preconditioning cycles were dismissed from the stress record (the finally fitted region is indicated in figure 4).

$$\sigma(t) = \int_0^t \overline{G}(t-\tau)\,\frac{dT^e(\lambda)}{d\lambda}\,\frac{d\lambda(\tau)}{d\tau}\,d\tau \tag{3}$$

The reduced stress relaxation function $\overline{G}(t)$ is given by a five-terms Prony series like in [34]:

$$\overline{G}(t) = g_\infty + \sum_{i=1}^{5} g_i\, e^{-t/\tau_i} \tag{4}$$

normalized such that:

$$\overline{G}(0) = g_\infty + \sum_{i=1}^{5} g_i = 1 \tag{5}$$

The relaxation time constants were fixed *a priori* to ensure the uniqueness of the fitted function $\overline{G}(t)$ [58]. Particularly, they were taken in decades: $\tau_1 = 0.01\ s$, $\tau_2 = 0.1\ s$, $\tau_3 = 1\ s$, $\tau_4 = 10\ s$ and $\tau_5 = 100\ s$ as in [32]. This allows a better understanding of the progress of relaxation through the different time scales.[1]

The elastic response function, $T^e(\lambda)$, provides the instantaneous stress response to a step increase in the uniaxial stretch λ and was formulated here using fully incompressible hyperelastic models. Four SED functions were tried: a polynomial function with 5 terms[2], Ψ_{pol}, the first order Ogden model, Ψ_{Og}, the GOH model [19], Ψ_{GOH}, in its isotropic version, and a combination of a neo-Hookean model and an exponential one, Ψ_{exp} (see table 1).

As explained in [13], the raw stress record, $\overline{\sigma}$, was treated in two steps:

1. At the beginning of the test, the upper platen might not be in full contact with the sample, causing a zero or even a positive initial slope in the stress-stretch curve of some samples, thus resulting in a spurious toe region. This produced certain numerical problems in the fitting of the experimental stress. Therefore, this spurious toe region was eliminated, with an iterative algorithm designed in [13]. Please refer to that work for further details.

[1] It must be noted that g_i is approximately the proportion of stress relaxed between τ_{i-1} and τ_i.
[2] It includes polynomial functions with less number of terms if any fitted constant is zero.

Table 1: SED functions and the corresponding elastic response functions.

SED	Elastic response function
$\Psi_{\text{pol}} = C_{10}(I_1-3) + C_{01}(I_2-3)+$	$T^e_{\text{pol}} = 2C_{10}\,(\lambda^2 - \frac{1}{\lambda}) + 2C_{01}\,(\lambda - \frac{1}{\lambda^2}) + 6C_{11}\,(\lambda^3 - \lambda^2 - \lambda+$
$+C_{11}(I_1-3)(I_2-3)+$	$+\frac{1}{\lambda} + \frac{1}{\lambda^2} - \frac{1}{\lambda^3}) + 4C_{20}\,(\lambda^4 - 3\lambda^2 + \lambda + \frac{3}{\lambda} - \frac{2}{\lambda^2})+$
$+C_{20}(I_1-3)^2 + C_{02}(I_2-3)^2$	$+4C_{02}\,(2\lambda^2 - 3\lambda - \frac{1}{\lambda} + \frac{3}{\lambda^2} - \frac{1}{\lambda^4})$
$\Psi_{\text{Og}} = \frac{\mu}{\alpha}(\lambda_1^\alpha + \lambda_2^\alpha + \lambda_3^\alpha - 3)$	$T^e_{\text{Og}} = \mu\,(\lambda^\alpha - \frac{1}{\lambda^{\frac{\alpha}{2}}})$
$\Psi_{\text{GOH}} = C_{10}(I_1-3) + \frac{k_1}{2k_2}[e^{k_2(I_1-3)^2} - 1]$	$T^e_{\text{GOH}} = 2(C_{10} + k_1(\lambda^2 + \frac{2}{\lambda} - 3)\,e^{k_2(\lambda^2+\frac{2}{\lambda}-3)^2})\,(\lambda^2 - \frac{1}{\lambda})$
$\Psi_{\text{exp}} = C_{10}(I_1-3) + \frac{k_1}{k_2}[e^{k_2(I_1-3)} - 1]$	$T^e_{\text{exp}} = 2(C_{10} + k_1\,e^{k_2(\lambda^2+\frac{2}{\lambda}-3)^2})\,(\lambda^2 - \frac{1}{\lambda})$

2. The record was filtered using a moving average filter to improve the shape of the curve.

The resulting stress record, named here $\tilde{\sigma}$, was fitted to the analytical stress record, σ, given through equation (3) by using a least squares method that minimizes the following quadratic error:

$$e = \sum_{i=1}^{N} \left(\tilde{\sigma}(t_i) - \sigma(t_i)\right)^2 \tag{6}$$

where N is the total number of points recorded during the relaxation test and t_i is the time elapsed since the beginning of the test at point i. As explained in [13], this least squares method is sensitive to the initial guess in nonlinear problems like this. For this reason, the optimization was performed in two steps. First a genetic algorithm was used to find a minimum of the quadratic error, e, which was used as the initial guess in the second step: the least squares optimization. The genetic algorithm guarantees that the minimum is searched in the entire domain, not only locally around the initial guess. However, genetic algorithms are heuristic methods and the minimum does not necessarily fulfill the optimality condition. This condition was met in the second step, which was a local search around the minimum found in the first step. The Trust Region Reflective algorithm implemented in Matlab was used for this local search. The goodness of the least squares fitting was evaluated by means of the coefficient of variation, CV:

$$CV(\%) = \frac{\sqrt{\frac{\sum_{i=1}^{N}\left(\sigma(t_i) - \tilde{\sigma}(t_i)\right)^2}{N}}}{\mu_{\tilde{\sigma}}} \times 100 \tag{7}$$

where $\mu_{\tilde{\sigma}}$ is the mean value of the temporal record $\tilde{\sigma}(t_i)$.

2.3. Data fitting algorithm: internal variables viscoelastic (IVV) model

With the internal variables viscoelastic (IVV) model, the structure of the algorithm is the same that in the previous section, though with different equations. This formulation was proposed in [25] and has been used to model isotropic materials, along with an extension, proposed to model fibre-reinforced materials [26]. In the isotropic version [25], the SED is decomposed in three terms:

$$\Psi_{IVV} = \Psi^{\infty}_{vol}(J) + \Psi^{\infty}_{iso}(\bar{\mathbf{C}}) + \sum_{j=1}^{m} \Upsilon_j \left(\bar{\mathbf{C}}, \Gamma_j\right) \tag{8}$$

describing the first two terms, respectively, the volumetric elastic response and the isochoric elastic response as $t \to \infty$ or in sufficiently slow processes. The summation is the dissipative potential, responsible for the viscoelastic behaviour, and depends on the isochoric deformation through the modified right Cauchy-Green tensor, $\bar{\mathbf{C}} = \bar{\mathbf{F}}^T\bar{\mathbf{F}}$, being $\bar{\mathbf{F}} = J^{-1/3}\mathbf{F}$ the modified deformation gradient tensor, $\mathbf{F}$ the deformation gradient tensor and J the volume ratio. Thus, the volumetric response remains fully elastic, with no contribution in the dissipative term. Γ_j are the strain-like internal variables. The well-known relation $\mathbf{S} = 2\frac{\partial \Psi_{IVV}}{\partial \mathbf{C}}$ provides the second Piola-Kirchhoff stress tensor, which takes the form:

$$\mathbf{S} = \mathbf{S}^{\infty}_{\text{vol}} + \mathbf{S}^{\infty}_{\text{iso}} + \sum_{j=1}^{m} \mathbf{Q}_j \tag{9}$$

with $\mathbf{S}^{\infty}_{\text{vol}}$ and $\mathbf{S}^{\infty}_{\text{iso}}$ the fully elastic volumetric and isochoric contributions to the second Piola-Kirchhoff stress tensor respectively, and $\mathbf{Q}_j$ the non-equilibrium stresses, whose evolution is given by:

$$\dot{\mathbf{Q}}_j + \frac{\mathbf{Q}_j}{\tau_j} = \dot{\mathbf{S}}_{\text{iso}\,j} \tag{10}$$

where τ_j is the j relaxation time, which plays the same role as τ_i in the QLV model, and $\mathbf{S}_{\text{iso}\,j}$ is the isochoric second Piola-Kirchhoff stress tensor, corresponding to the isochoric strain energy function $\Psi_{\text{iso}\,j}$ and responsible for the j relaxation process. The solution of the differential equation (10) for $t \in (0, T]$ is:

$$\mathbf{Q}_j = e^{-T/\tau_j}\,\mathbf{Q}_{j\,0^+} + \int_{t=0^+}^{t=T} e^{-(T-t)/\tau_j}\,\dot{\mathbf{S}}_{\text{iso}\,j}(t)\,dt \tag{11}$$

where $\mathbf{Q}_{j\,0^+}$ is the instantaneous stress response appearing at $t = 0^+$. The tensors $\mathbf{S}_{\text{iso}}\,j$ are defined next. If the viscoelastic medium is composed of identical polymer chains (or collagen fibres in the case of adipose tissue), $\Psi_{\text{iso}\,j}$ is replaceable by the strain energy function $\Psi^{\infty}_{\text{iso}}$ [25], by assuming:

$$\Psi_{\text{iso}\,j}(\bar{\mathbf{C}}) = \beta_j^{\infty}\ \Psi_{\text{iso}}^{\infty}(\bar{\mathbf{C}}) \tag{12}$$

or equivalently

$$\mathbf{S}_{\text{iso}\,j} = \beta_j^{\infty}\ \mathbf{S}_{\text{iso}}^{\infty}(\bar{\mathbf{C}}) \tag{13}$$

The β_j^{∞} constants are dimensionless strain energy factors, which play the same role as g_i in the QLV model. $\mathbf{S}_{\text{iso}}^{\infty}$ can be obtained in two different ways, depending on the structure of the SED function. If this is expressed in terms of the invariants of the modified Cauchy-Green tensors, $\bar{I}_i$ with $i = 1, 2, 3$ (polynomial, exponential and GOH), then:

$$\mathbf{S}_{\text{iso}}^{\infty} = J^{-2/3}\mathbb{P} : \bar{\mathbf{S}}^{\infty} \tag{14}$$

where $\mathbb{P} = \mathbb{I} - 1/3\ \mathbf{C}^{-1} \otimes \mathbf{C}$ is the projection tensor, $\mathbb{I}$ is the fourth-order unit tensor, and $\bar{\mathbf{S}}^{\infty}$ is the fictitious second Piola-Kirchhoff stress tensor, given by:

$$\bar{\mathbf{S}}^{\infty} = 2\left(\frac{\partial \Psi_{\text{iso}}^{\infty}}{\partial \bar{I}_1} + \bar{I}_1 \frac{\partial \Psi_{\text{iso}}^{\infty}}{\partial \bar{I}_2}\right)\mathbf{I} - 2\,\frac{\partial \Psi_{\text{iso}}^{\infty}}{\partial \bar{I}_2}\ \bar{\mathbf{C}} \tag{15}$$

In case the SED function depends on the modified principal stretches, $\bar{\lambda}_a$, $\mathbf{S}_{\text{iso}}^{\infty}$ can be directly calculated as:

$$\mathbf{S}_{\text{iso}}^{\infty} = \sum_{a=1} \frac{1}{\lambda_a} \frac{\partial \Psi_{\text{iso}}^{\infty}(\bar{\lambda}_a)}{\partial \lambda_a} \hat{N}_a \otimes \hat{N}_a \tag{16}$$

being $\hat{N}_a$ the direction of the principal stretches.

The Cauchy stress tensor is finally obtained from equation (9), by using the relation $\boldsymbol{\sigma} = J^{-1}\mathbf{F}\mathbf{S}\mathbf{F}^T$:

$$\boldsymbol{\sigma} = \boldsymbol{\sigma}_{\text{vol}}^{\infty} + \boldsymbol{\sigma}_{\text{iso}}^{\infty} + \sum_{j=1}^{m} J^{-1}\mathbf{F}\mathbf{Q}_j\mathbf{F}^T = \boldsymbol{\sigma}^{\infty} + \sum_{j=1}^{m} J^{-1}\mathbf{F}\mathbf{Q}_j\mathbf{F}^T \tag{17}$$

The formulation presented above is intended for the general treatment of compressible materials. For incompressible materials, as assumed here, $J = 1$, the modified tensors are equal to the original ones ($\bar{\mathbf{F}} = \mathbf{F}$, $\bar{\mathbf{C}} = \mathbf{C}$) and the volumetric SED is equal to zero. In these terms, $\boldsymbol{\sigma}_{\text{vol}}^{\infty}$ is replaced by a hydrostatic pressure, which must be worked out from the boundary conditions. Under these premises, $\boldsymbol{\sigma}^{\infty}$ turns out to be:

$$\boldsymbol{\sigma}^{\infty} = \begin{bmatrix} 0 & 0 & 0 \\ 0 & 0 & 0 \\ 0 & 0 & T^e(\lambda) \end{bmatrix} \tag{18}$$

if the load is applied in direction 3, with $T^e(\lambda)$ the same function given in table 1 for the different SED functions.

For the non-equilibrium forces $\mathbf{Q}_j$, 5 terms were selected as in the QLV model (i.e. $j = 1, ..., 5$). As previously, the relaxation time constants, τ_j, were fixed *a priori* to ensure the uniqueness of the fitted set of constants and taken in the same decades: $\tau_1 = 0.01\ s$, $\tau_2 = 0.1\ s$, $\tau_3 = 1\ s$, $\tau_4 = 10\ s$ and $\tau_5 = 100\ s$.

Also, the same four SED functions used with the QLV model were used with the IVV model. With the stretch temporal evolution, $\lambda = \lambda(t)$, given by Eq. (2), $\boldsymbol{\sigma}^{\infty}$ can be calculated through Eq. (18). Additionally, using Eqs. (13)-(16) $\mathbf{S}_{\mathrm{iso}\,j}$ can be calculated to be used in Eq. (11). The derivative and integral in (11) were obtained following the algorithm presented in [25] (pages 290-293).

The preconditioning cycles were not considered in the fitting algorithm. For the implementation of these equations, the algorithm proposed in [27] has been followed. Please refer to that work for further details.

The treatment of the experimental stress record (elimination of the spurious toe region and filtering of the record), the least squares fitting method and the evaluation of the fitting goodness through the CV were exactly the same that with the QLV model.

2.4. Performed tests

Following the test protocol and the fitting algorithm presented before, the viscoelastic properties of the human abdominal fat were determined. The number of specimens used for each strain rate was: 47 for $50\%/s$, 45 for $60\%/s$ and 46 for $70\%/s$.

First, the four proposed SED functions were compared to check which one fitted best the experimental curves for each viscoelastic model. The goodness of fit was assessed through CV (eq.(7)) and the mean CV was calculated for each SED function using the whole set of specimens ($47 + 45 + 46$). The lowest CV determines the best SED function. Then, the best model was validated by randomly selecting 10% of the specimens of each strain rate (5+4+5), to make up three subsets called *validation subsets*. The constants fitted for each of these subsets were compared with the medians and interquartile ranges (IQR) of the constants fitted for the remaining 90% of the corresponding strain rate, or *control subset*.

The validity of both viscoelastic schemes, QLV and IVV, was then verified, again for the best SED function. This validity is based on the independence of the fitted material constants with the strain rate. So, the different sets of

constants for each strain rate were compared using a statistical test to detect significant differences. The whole set of specimens was used in this comparison.

3. Results

3.1. Goodness of fit of the hyperelastic models with the QLV model

Figure 5 compares a typical experimental stress record, $\tilde{\sigma}$, with the fitting curves for each of the proposed SED functions. In figure 6 a detail of the experimental and fitted stresses obtained during the loading ramp can be seen.

The mean of the CVs, obtained for the whole set of specimens is presented in table 2 for each SED function. The CVs were evaluated for the whole test and for the loading ramp separately.

The polynomial one is a general hyperelastic model, in the sense that it can lead to other models, differently named in the literature, for example, the Mooney-Rivlin model if $C_{11} = C_{20} = C_{02} = 0$. The fit with the polynomial model was carried out without imposing restrictions to the material constants. For this reason, some of those constants resulted zero for certain specimens. Besides, those zero constants were not systematically the same for all the specimens. Thus, the average model resulted in a five terms polynomial model, but the individual models for each specimen could be different. Some of them were better modelled with the Mooney-Rivlin scheme or other particular forms of the polynomial model. In other words, the five terms polynomial model does not represent the behaviour of all the specimens on a general basis and can be considered inconsistent, despite producing the lowest CV.

The same occurred to the isotropic GOH model. In many specimens, the fit led to $k_2 = 0$. In the limit:

$$\lim_{k_2 \to 0} \Psi_{GOH} = C_{10}(I_1 - 3) + \frac{k_1}{2}(I_1 - 3)^2 \tag{19}$$

which is a particular case of the 5 terms polynomial SED function. This is the reason why the GOH and the polynomial models fitted the experimental curves very similarly. Thus, the isotropic GOH model was also considered inconsistent to model the adipose tissue. In view of the foregoing and the average CV, the Ogden model was selected as the best one (most consistent) to represent the behaviour of the adipose tissue from those ones chosen *a priori*.

Table 2: Coefficient of variation of the fitting with the QLV model and the different SED functions.

Model	Whole test CV (%)	Loading ramp CV (%)
Exponential	4.16	19.88
Ogden	4.05	18.70
GOH	3.06	11.49
Polynomial	2.92	10.67

Table 3: Median and IQR of the QLV constants for the different groups, using the Ogden model and the *control subsets* (90% of the specimens of each group).

Strain rate	Quartile	μ (kPa)	α	g_1	g_2	g_3	g_4	g_5	g_∞	$CV_{Q1\ or\ Q3}$ (%)
	Q1	3.260	7.632	0.533	0.190	0.039	0.017	0.017	0.013	69.2%
50% /s	Median	4.780	8.485	0.654	0.222	0.049	0.024	0.023	0.018	—
	Q3	9.308	9.625	0.719	0.316	0.071	0.034	0.033	0.022	229.3%
	Q1	2.721	7.358	0.558	0.176	0.038	0.018	0.017	0.013	84.7%
60% /s	Median	6.529	8.361	0.674	0.218	0.049	0.023	0.024	0.017	—
	Q3	10.467	9.382	0.730	0.316	0.063	0.031	0.030	0.023	229.8%
	Q1	3.093	7.456	0.545	0.195	0.042	0.021	0.020	0.014	66.2%
70% /s	Median	4.546	8.437	0.616	0.242	0.049	0.026	0.025	0.018	—
	Q3	8.544	9.501	0.708	0.285	0.067	0.038	0.036	0.027	324.4%

3.2. Validity of the QLV model. Part I

The combination QLV+Ogden was validated in two ways. In this section, the specimens of the *validation subsets* were compared with those of the *control subsets*. Table 3 shows the medians and IQRs of each constant corresponding to these *control subsets*. It was found that 52% of the constants fitted for the *validation subsets* lied in the IQRs presented in the table. This result is logical, since, theoretically, 50% of the specimens should lie within the IQR.

Next, it was checked whether the medians given in table 3 fit well the results of the *validation subsets*. Each strain rate group was checked separately. So, the constants of each median were used in equation (3) to provide the stress evolution $\sigma_{med}(t)$, which should represent an average stress evolution at a certain strain rate. This evolution was compared at every instant t_i with the experimental stress record of specimen j of the *validation subset*, $\tilde{\sigma}_j$, to give the following coefficient of variation:

$$CV_j\,(\%) = \frac{\sqrt{\frac{\sum_{i=1}^{N}\left(\sigma_{med}(t_i) - \tilde{\sigma}_j(t_i)\right)^2}{N}}}{\mu_{\tilde{\sigma}}} \times 100 \tag{20}$$

The mean of CV_j for all the specimens of the *validation subsets* (including the three strain rates altogether) was 85.9%. This value is so high due to the wide scattering of the results. To estimate this dispersion let us define the following coefficient of variation:

$$CV_{Q1}(\%) = \frac{\sqrt{\frac{\sum_{i=1}^{N}\left(\sigma_{Q1}(t_i) - \sigma_{med}(t_i)\right)^2}{N}}}{\mu_{\sigma_{med}}} \times 100 \tag{21}$$

where the stress evolution obtained by using the set of constants Q1, σ_{Q1}, is again compared with $\sigma_{med}(t)$, like in

(20). An analogous expression is used to define CV_{Q3}. The values of these coefficients are shown in table 3 for each strain rate. It can be noted that CV_{Q3} is especially high, which is due to some abnormally rigid specimens. However, the mean of CV_j of the *validation subsets* (85.9%) is very close to CV_{Q1}, and lies within the normal dispersion of the mechanical properties of living tissues.

3.3. Validity of the QLV model. Part II

In this section, the validity of the viscoelastic formulation was proved by checking if the fitted constants were independent of the strain rate. For this purpose, the whole set of specimens were used in a multivariate analysis of variance. The categorical independent variable (IV) was the strain rate with three levels: $50\%/s$, $60\%/s$ and $70\%/s$. The dependent continuous variables (DVs) were the seven QLV constants: μ, α, of the Ogden model; and g_1, g_2, g_3, g_4 and g_5 of the Prony series. The constant g_∞ was not included in the statistical analysis because it is a linear combination of the other Prony constants, g_i, due to the normalization condition (5).

To check if the material constants were independent of the strain rate, a non parametric MANOVA (NMANOVA) test was performed, given that the stress does not vary linearly with the constant α[1]. Moreover, to apply a parametric MANOVA some assumptions, such as multinormality, need to be checked beforehand. This multinormality was checked for each independent group using the test developed by Cardoso de Oliveira and Ferreira [6]. This test was not significant for the 50% /s group ($p = .098$) and 60% /s group ($p = .160$), but it was for the 70% /s group ($p < .001$) and, thus, multinormality was violated, making it necessary to perform a non-parametric MANOVA (NMANOVA).

The NMANOVA test performed in this work is a multivariate extension of the Kruskal-Wallis test, developed by Katz and McSweeney [31]. Initially, the test was carried out for the 7 aforementioned DVs. No significant differences were found for the three groups compared ($p = .819$). Nonetheless, some authors state that the MANOVA type tests are only indicated if the dependent variables are correlated, but not so strongly correlated ($|R| > .85$) that multicollinearity may exist [15, 22]. In this case, constants g_1 and g_2 were strongly correlated and the same occurred to g_3, g_4 and g_5 (Spearman $|R| > .85$ in both cases). So, to be sure of the previous conclusion, the test was repeated after eliminating the correlated variables, that is, for the following 4 DVs: μ, α, g_1 and g_3. The conclusion was the same: there were no statistical differences between the groups ($p = .997$). Therefore, the material constants of the QLV model can be considered independent of the strain rate.

3.4. Goodness of fit of the hyperelastic models with the IVV model

The same analysis presented before was repeated for the IVV model. Figure 7 compares one of the experimental stress record, $\tilde{\sigma}$, the same shown in figures 5 and 6, with the fitting curves for each of the proposed SED functions. In

[1] For this reason, the median of α represents the sample better than the mean.

Table 4: Coefficient of variation of the fitting with the IVV model and the different SED functions.

Model	Whole curve CV (%)	Loading ramp CV (%)
Exponential	3.81	17.66
Ogden	3.77	16.99
GOH	3.04	11.36
Polynomial	3.14	12.27

figure 8 a detail of the experimental and fitted stresses obtained during the loading ramp can be seen.

The mean of the CVs obtained for the whole set of specimens is presented in table 4 for each SED function. Again, the CV was evaluated for the whole test and for the loading ramp separately.

As in the QLV model, the fit with the polynomial and the isotropic GOH SED functions produced some zero constants in certain specimens. For the same reason discussed before, the Ogden model was selected as the best one to represent the behaviour of the adipose tissue from those chosen *a priori*.

3.5. Validity of the IVV model. Part I

As in sections 3.2 and 3.3, the combination IVV+Ogden was validated in two ways. First, by comparing the constants fitted for the *validation subsets* with those of the *control subsets*, whose medians and IQRs are presented in table 5. Now, 46% of the constants fitted for the *validation subsets* lied within the IQRs presented in the table.

The coefficients CV_{Q1} and CV_{Q3} defined in section 3.2 are also given in table 5 for this model. The average of CV_j for the *validation subsets* was 94.7% in this case, a little higher than the values of CV_{Q1}.

3.6. Validity of the IVV model. Part II

In this section, the validity of the viscoelastic model was proved by checking if the fitted constants were independent of the strain rate. Again, the whole set of specimens were used in a multivariate analysis of variance. A NMANOVA test was also carried out since the stress does not vary linearly with the constant α. Moreover, multinormality was checked for each independent group using the test developed by Cardoso de Oliveira and Ferreira [6]. This test was not significant for the 50% /s group ($p = .534$) and 70% /s group ($p = .205$), but it was for the 60% /s group ($p = .003$) and, thus, multinormality was violated, making it necessary to perform a non-parametric MANOVA (NMANOVA). The strain rate was the categorical IV, with three levels ($50\%/s$, $60\%/s$ and $70\%/s$); and 7 DVs: μ, α, $\beta_1^\infty, \beta_2^\infty, \beta_3^\infty, \beta_4^\infty$ and β_5^∞. The correlation between the DVs was checked, but they were not highly correlated (Spearman $|R| < .85$), so that all of them were considered in the analysis.

The NMANOVA test developed by Katz and McSweeney [31] showed no significant differences between the three groups compared ($p = .314$). Therefore, the material constants could be considered independent of the strain rate.

Table 5: Median and IQR of the IVV constants for the different groups, using the Ogden model and the *control subsets* (90% of the specimens of each group)

Strain rate	Quartile	μ (kPa)	α	β_1^∞	β_2^∞	β_3^∞	β_4^∞	β_5^∞	$CV_{Q1\ or\ Q3}$ (%)
	Q1	0.067	7.345	39.216	9.966	3.170	1.682	1.715	63.3 %
50% /s	Median	0.102	8.467	69.022	13.221	3.939	1.993	1.910	—
	Q3	0.162	9.527	106.125	20.079	4.947	2.491	2.178	168.1 %
	Q1	0.066	6.964	43.159	9.702	3.278	1.672	1.746	71.8 %
60% /s	Median	0.119	8.252	67.712	12.734	3.837	1.957	1.940	—
	Q3	0.197	9.424	101.241	18.395	4.933	2.383	2.237	191.0 %
	Q1	0.069	7.110	43.140	8.543	3.208	1.689	1.791	68.1 %
70% /s	Median	0.121	8.218	62.563	11.315	3.688	2.024	1.965	—
	Q3	0.169	9.293	94.787	17.984	4.247	2.539	2.296	137.0 %

4. Discussion

The presence of a toe region, typical of soft tissues; can be observed in the experimental curves of figures 5 and 6. In normal toe regions the slope of the stress record is initially very small and increases very slightly, for example, in the articular discs of the temporomandibular joint [13]. However, in the present case, the toe region was not very wide and the loading ramp was quickly noticed by an increase in the compression stress. The relaxation was very quick, with a high percentage (around 70%) of the stress relaxed just a few seconds after the peak and more than 90% of the peak stress relaxed after 15 minutes. Comparing these stress relaxation curves with those obtained by Miller-Young et al. [39], who tested specimens of the human calcaneal fat pad in compression, the peak stress of the present work was of the same order of magnitude and, in both, 75% of the stress was relaxed within the first minute.

It has also been observed, as pointed out by Carniel et al. [8], that the influence of the strain rate on the ratio between the peak stress and the non-relaxed stress (the stress remaining as $t \to \infty$) is very important. The higher the strain rate, the faster the loading ramp and, therefore, the larger is the difference between those two stresses. These authors also emphasised the importance of relaxation during the loading ramp, and the error that can be committed by assuming that the test is an ideal relaxation test (strain applied in a step increase) and fitting only the relaxation phase, after the peak stress is reached. The whole test, including the ramp and the relaxation therein, must be accounted for in the fit, as done in the present study.

It can be seen in figures 5 and 6, that the fit with the QLV model was quite accurate for the selected specimen. In fact, it was equally accurate for all the specimens and very similar for the four SED functions. It can be also noticed that the isotropic GOH and the 5 terms polynomial models fit the experimental curve slightly better than the Ogden and exponential functios, although not too much.

For the QLV model, the best SED function in terms of goodness of fit, CV, was the polynomial one, closely followed by the GOH function, and a bit farther by the Ogden and exponential functions, in this order (see table 2). In all cases, the CV was quite low for the fit of the complete stress record. Nonetheless, as discussed before, the polynomial and GOH SED functions were dismissed since they failed to fit all the specimens with the same general equation. For that reason, the Ogden model was eventually selected as the best SED function from those tried in this work.

The high values obtained for the median of g_1 and g_2 (see table 3), corresponding to the relaxation times $\tau_1 = 0.01$ and $\tau_2 = 0.1$, highlight the fast relaxation of the specimens. The sum of both (around 90%) represents the percentage of the peak stress relaxed up to tenths of a second.

Regarding the IVV model, it can be seen in figures 7 and 8 that the fit was also very accurate for the selected specimen, which was representative of the general trend. Though not shown, it was equally accurate for all the specimens. The four SED functions produced similar results, but the best fitting was achieved with the GOH function, closely followed by the polynomial function and a bit farther away by the Ogden and exponential ones, in this order, as can be deduced from CV (see Table 4).

The goodness of the fit, in terms of CV, was slightly better with the IVV model than with the QLV model for all the SED functions, except for the polynomial model, in which case it was only slightly worse (compare Tables 2 and 4). As in the QLV model, both the polynomial and GOH functions failed to fit all the specimens with the same general equation and, thus, the Ogden model was finally selected as the best (most consistent) SED function for the IVV model, from those tried in this work.

The parameters β_j^∞ are analogous to the Prony constants g_j in the IVV model and are related to the percentage of stress relaxed up to the relaxation time τ_j. It can be seen in table 5 how the median of β_j^∞ decrease with j, e.g. the relaxation occurred very quickly as was also deduced from the QLV model.

The validity of both schemes, QLV and IVV, in combination with the Ogden model was proven in two ways. First, by randomly selecting 10% of the specimens of each strain rate (*validation subsets*) and comparing their constants with those of the remaining 90% of the corresponding strain rate (*control subsets*). So, it was found that around 50% of the former constants were within the IQR of the latter ones, as expected.

Moreover, the median set of constants obtained for the *control subset* of each strain rate was used to define an average stress evolution, σ_{med}, which was compared with the experimental stress records of the corresponding *validation subset*. The individual difference between those stress records was measured by a coefficient of variation CV_j (see Eq. (20)), which was around 90% in average. This high value is only partially explained by the intrinsic dispersion of the mechanical properties of living tissues. In fact, it is so high due to the presence of some abnormally

Table 6: Median and interquartile range of the IVV constants for the human abdominal adipose tissue using the Ogden model and the whole set of specimens.

Quartile	μ (kPa)	α	β_1^∞	β_2^∞	β_3^∞	β_4^∞	β_5^∞
Q1	0.069	7.105	43.995	8.993	3.221	1.681	1.732
Median	0.115	8.215	66.663	12.761	3.836	1.988	1.950
Q3	0.176	9.437	99.0763	18.872	4.790	2.447	2.238

rigid specimens in the *validation subsets*, being the stresses in those specimens considerably higher than in the median stress record.

The presence of abnormally rigid specimens was not exclusive to the *validation subsets* and could also be seen in the *control subsets*, whose dispersion was very wide, as demonstrated by the high values of CV_{Q3}. The explanation for the existence of these rigid specimens is unknown and it should be further investigated whether it is due to a particular composition or microstructure.

The second way to validate the viscoelastic models consisted in checking that the material constants were independent of the strain rate applied in the test. Given that the IVV model produced a slightly better fitting than QLV model, it can be concluded that the IVV model with an Ogden SED function for the elastic response was the best choice to characterise the abdominal adipose tissue, from the models tried in this work. Therefore, and due to the independence of the strain rate, the median and IQR of each constant were calculated for the whole set of specimens and are presented in table 6.

The goodness of fit of the IVV model was just slightly better, but it has other conceptual advantages with respect to the QLV model that need to be mentioned. First, it is a fully non-linear model, while QLV is quasi-linear, in the sense that it assumes the validity of the Boltzmann superposition principle [17], not needed in the IVV model. Second, it is valid for three dimensional load cases, while the QLV model, in the version used here, is only valid for uniaxial stress states. Some 3D extensions have been proposed (see [54] for example), but they involved a great number of constants. Apart from this, both models uncouple the viscous and elastic parts of the behaviour; the QLV model with a multiplicative decomposition of the stress and the IVV model with an additive decomposition of the SED function, with a specific term for the energy dissipation, which is more meaningful from a physical point of view.

In view of the values obtained for g_∞, the length of experiments, 15 minutes, seems enough to capture the stress relaxation of the specimens. g_∞ can be interpreted as the proportion of stress that remains to be relaxed after the last relaxation time, $\tau_5 = 100$ s in this case. Table 3 shows that g_∞ is around 0.02, so that only 2% of the stresses remain to be relaxed after the first minutes.

As stated in section 2.1 the specimens were frozen during 1 day at most. Freezing of tissues may damage their

microstructure under certain circumstances, compromising their structural integrity and altering the measured mechanical properties. The influence of freezing storage time at $-20°C$ on the viscoelastic behaviour of the articular disc has been recently analyzed [5] to find that it has no effect if the storage time is shorter than one month. To the authors' knowledge, no similar study has been performed on adipose tissue, which could have a different sensitivity to freezing. However, the storage time is so much shorter in this case that no influence is expected.

The analyzed specimens were extracted from the same patient and this is a limitation of the study, but it was justified in a pilot study like the present one for the following reason. In a previous work [4], the viscoelastic properties of the adipose tissue of two patients were compared, finding significant differences between them. That result highlights the specificity of the mechanical properties of the adipose tissue of each individual. The main objective of the present study was validating the use of certain viscoelastic models, which implied comparing the material constants fitted for different strain rates. So, the only variable whose effect was of interest was the strain rate and other sources of scattering, such as inter-individual differences, should be eliminated from the statistical analysis, otherwise they could have hidden the main effect of the strain rate.

Those inter-individual differences might be due to multiple factors, such as age, collagen content, body mass index, etc., which might also have an influence on the validity of the proposed model. The origin of inter-individual differences is still unknown and that complicates the design of experiments. Thus, future studies must tackle two different topics for a complete characterization of the viscoelastic behaviour of the adipose tissue: 1) to prove the validity of the present model on a general basis, by proving the independence of the constants with the strain rate for a significantly larger sample of individuals and 2) to identify the origin of inter-individual differences.

Finally, it is important to note the limited relevance of knowing the viscoelastic properties of the adipose tissue in clinical situations. In most of the applications where this tissue is involved and particularly in the deformation of the reconstructed breast, the dynamic effects are normally irrelevant. The hyperelastic function is the key part of the model, because it determines the organ shape under static loads, while the viscoelastic part only affects dynamic behaviour, in vibrations or impacts, for example. Notwithstanding the foregoing, the viscoelastic part is important in experimental tests, since they are performed under finite strain rates to reduce the experimentation time. In other words, the viscoelastic behaviour must be taken into account in the experimental tests, but mainly to be able to extract the long-term behaviour, given by the hyperelastic function, which is what matters from a clinical point of view.

5. Conclusion

In the present work, the viscoelastic behaviour of the human adipose tissue has been investigated. Stress relaxation tests at different strain rates were carried out and fitted with two different models, the quasi-linear viscoelastic and

the internal variables viscoelastic models. The same four SED functions were used to describe the elastic response in both cases. It was found that all of them provided a good fit of the experimental results, being the internal variables viscoelastic model with an Ogden SED function the most consistent option. Moreover, the validity of both viscoelastic models was checked by statistically comparing the constants fitted for different strain rates and finding no significant differences between those fitted constants.

Conflict of interest statement

The authors declare that they have no conflict of interest.

Acknowledgements

The authors gratefully acknowledge the research support from the Spanish *'Ministerio de Economía y Competitividad'* through the research project DPI2011-28080, *'Modelado numérico de un proceso de reconstrucción mamaria'*.

References

[1] K. D. Allen and K. A. Athanasiou. Viscoelastic characterization of the porcine temporomandibular joint disc under unconfined compression. *Journal of Biomechanics*, 39(5):312–322, 2006.

[2] F. S. Azar, D. N. Metaxas, and M. D. Schnall. A deformable finite element model of the breast for predicting mechanical deformations under external perturbations. *Academic Radiology*, 8:965–975, 2001.

[3] M. B. Bennett and R. F. Ker. The mechanical properties of the human subcalcaneal fat pad in compression. *Journal of Anatomy*, 171:131–138, 1990.

[4] J. L. Calvo-Gallego. *Experimental Characterisation of Breast Tissues and its Application to a Numerical Model of a Healthy Breast*. PhD thesis, Universidad de Sevilla, 2017.

[5] J. L. Calvo-Gallego, M. S. Commisso, J. Domínguez, E. Tanaka, and J. Martínez-Reina. Effect of freezing storage time on the elastic and viscous properties of the porcine tmj disc. *Journal of the Mechanical Behaviour of Biomedical Materials*, 71:314–319, 2017.

[6] I. R. Cardoso de Oliveira and D. F. Ferreira. Multivariate extension of chi-squared univariate normality test. *Journal of Statistical Computation and Simulation*, 80(5):513–526, 2010.

[7] E. O. Carew, E. A. Talman, D. R. Boughner, and et al. Quasi-linear viscoelastic theory applied to internal shearing of porcine aortic valve leaflets. *Journal of Biomechanical Engineering*, 121:386–392, 1999.

[8] E. L. Carniel, C.G. Fontanella, C. Stefanini, and A.N. Natali. A procedure for the computational investigation of stress-relaxation phenomena. *Mechanics of Time-Dependent Materials*, 17(1):25–38, 2013.

[9] K. Chen and J. D. Weiland. Mechanical properties of orbital fat and its encapsulating connective tissue. *Journal of Biomechanical Engineering*, 133(6), 2011.

[10] K. Comley and N. Fleck. The high strain rate response of adipose tissue. In G. M. L. Gladwell, R. Moreau, H. Zhao, and N. Fleck, editors, *IUTAM Symposium on Mechanical Properties of Cellular Materials*, volume 12, pages 27–33. Springer, Netherlands, 2009.

[11] K. Comley and N. Fleck. The mechanical response of porcine adipose tissue. *ASME Journal of Biomechanical Engineering*, pages 1–30, 2009.

[12] K. Comley and N. Fleck. The toughness of adipose tissue: measurements and physical basis. *Journal of Biomechanics*, 43:1823–1826, 2010.

[13] M. S. Commisso, J. L. Calvo-Gallego, J. Mayo, and et al. Quasi-linear viscoelastic model of the articular disc of the temporomandibular joint. *Experimental Mechanics*, 56(7):1169–1177, 2016.

[14] M. S. Commisso, J. Martínez-Reina, J. Mayo, and et al. Numerical simulation of a relaxation test designed to fit a quasi-linear viscoelastic model for temporomandibular joint discs. *Proceedings of the Institution of Mechanical Engineers, Part H: Journal of Engineering in Medicine*, 227 (2):190–199, 2013.

[15] W. R. Dillon and M. Goldstein. *Multivariate analysis. Methods and applications*. John Wiley & Sons, USA, 1984.

[16] C. S. Drapaca, G. Tenti, K. Rohlf, and et al. A quasi-linear viscoelastic constitutive equation for the brain: application to hydrocephalus. *Journal of Elasticity*, 85:65–83, 2006.

[17] Y. C. Fung. *Biomechanics: Mechanical properties of living tissues*. Spinger-Verlag, New York, 1993.

[18] T. B. Gamage, R. Boyes, V. Rajagopal, and et al. Modelling prone to supine breast deformation under gravity loading using heterogeneous finite element models. In A. Wittek P. M. F. Nielsen and K. Miller, editors, *Computational Biomechanics for Medicine*, pages 29–38. Springer New York, 2012.

[19] T. C. Gasser, R. W. Ogden, and G. A. Holzapfel. Hyperelastic modelling of arterial layers with distributed collagen fiber orientations. *Journal of the Royal Society Interface*, 3:15–35, 2006.

[20] M. Geerligs, G. W. M. Peters, P. A. J. Ackermans, and et al. Linear vicoelastic behaviour of subcutaneous adipose tissue. *Biorheology*, 45:677–688, 2008.

[21] S. M. Haddad, E. Omidi, L. E. Flynn, and A. Samani. Comparative biomechanical study of using decellularized human adipose tissues for post-mastectomy and post-lumpectomy breast reconstruction. *Journal of the Mechanical Behaviour of Biomedical Materials*, 57:235–245, 2016.

[22] J. F. Hair, R. L. Tatham, R. E. Anderson, and et al. *Multivariate Data Analysis*. Prentice Hall, New Jersey, 1998.

[23] L. Han, J. H. Hipwell, B. Eiben, and et al. A nonlinear biomechanical model based registration method for aligning prone and supine MR breast images. *IEEE Transactions on Medical Imaging*, 33(3):682–694, 2014.

[24] L. Han, J. H. Hipwell, C. Tanner, and et al. Development of patient-specific biomechanical models for predicting large breast deformation. *Physics in Medicine and Biology*, 57:455–472, 2012.

[25] G. A. Holzapfel. *Nonlinear solid mechanics: A continuum approach for engineering*. Wiley, Chichester, England, 2000.

[26] G. A. Holzapfel and T. C. Gasser. A viscoelastic model for fiber-reinforced composites at finite strains: continuum basis, computational aspects and applications. *Computer Methods in Applied Mechanics and Engineering*, 190:4379–4403, 2001.

[27] G. A. Holzapfel, T. C. Gasser, and R. W. Ogden. A new constitutive framework for arterial wall mechanics and a comparative study of materials models. *Journal of Elasticity*, 61:1–48, 2000.

[28] T. Hopp, P. Baltzer, M. Dietzel, and et al. 2D/3D image fusion of X-ray mammograms with breast MRI: visualizing dynamic contrast enhacement in mammograms. *International Journal of Computed Assisted Radiology and Surgery*, 7:339–348, 2012.

[29] T. Hopp, M. Dietzel, P. Baltzer, and et al. Automatic multimodal 2D/3D breast image registration using biomechanical FEM models and intensity-based optimization. *Medical Image Analysis*, 17:209–218, 2013.

[30] T. Hopp, M. Holzapfel, N. Ruiter, and et al. Registration of X-ray mammograms and three-dimensional speed of sound images of the female breast. *SPIE Proceedings*, 7629:1–9, 2010.

[31] B. M. Katz and M. McSweeney. A multivariate Kruskal-Wallis test with post-hoc procedures. *Multivariate Behavioral Research*, 15:281–297,

1980.

[32] J. H. Koolstra, E. Tanaka, and T. M. G. J. van Eijden. Viscoelastic material model for the temporomandibular joint disc derived from dynamic shear test or strain relaxation tests. *Journal of Biomechanics*, 40:2330–2334, 2007.

[33] A. Lagares-Borrego, P. Gacto-Sanchez, P. Infante-Cossio, and et al. A comparison of long-term cost and clinical outcomes between the two-stage sequence expander/prosthesis and autologous deep inferior epigastric flap methods for breast reconstruction in a public hospital. *Journal of Plastic, Reconstructive and Aesthetic Surgery*, 69:196–205, 2016.

[34] M. J. Lamela, Y. Prado, P. Fernandez, and et al. Non-linear viscoelastic model for behavior characterization of temporomandibular joint discs. *Experimental Mechanics*, 51:1453–1440, 2011.

[35] A. Lapuebla-Ferri, A. Pérez del Palomar, J. Herrero, and et al. A patient-specific FE-based methodology to simulate prosthesis insertion during an augmentation mammoplasty. *Medical Engineering & Physics*, 33:1094–1102, 2011.

[36] E. Matros, C. R. Albornoz, S. N. Razdan, and et al. Cost-effectiveness analysis of implants versus autologous perforator flaps using the breast-q. *Plastic and Reconstructive Surgery*, 135:937–946, 2015.

[37] S. Matteoli, C. G. Fontanella, E. L. Carniel, and et al. Investigation on the viscoelastic behaviour of a human healthy heel pad: In vivo compression tests and numerical analysis. *Proceedings of the Institution of Mechanical Engineers, Part H: Journal of Engineering in Medicine*, 227 (3):216–223, 2013.

[38] T. Mertzanidou, J. Hipwell, S. Johnsen, and et al. MRI to X-ray mammography instensity-based registration with simultaneous optimisation of pose and biomechanical transformation parameters. *Medical Image Analysis*, 18:674–683, 2014.

[39] J. E. Miller-Young, N. A. Duncan, and G. Baroud. Material properties of the human calcaneal fat pad in compression: experiment and theory. *Journal of Biomechanics*, 35:1523–1531, 2002.

[40] A. N. Natali, C. G. Fontanella, and E. L. Carniel. A numerical model for investigating the mechanics of calcaneal fat pad region. *Journal of the Mechanical Behaviour of Biomedical Materials*, 5 (1):216–223, 2012.

[41] P. Pathmanathan, D. Gavaghan, J. Whiteley, and et al. Predicting tumour location by simulating large deformations of the breast using a 3-D finite element model and nonlinear elasticity. *Medical Image Computing and Computer-Assisted Intervention*, 2:217–224, 2004.

[42] A. Pérez del Palomar, B. Calvo, J. Herrero, and et al. A finite element model to accurately predict real deformations of the breast. *Physics in Medicine and Biology*, 30:1089–1097, 2008.

[43] S. Pianigiani, L. Ruggiero, and B. Innocenti. An anthropometric-based subject-specific finite element model for the human breast for predicting large deformations. *Frontiers in Bioengineering and Biotechnology*, 3(201):1–9, 2015.

[44] V. Rajagopal, A. Lee, J. H. Chung, and et al. Towards tracking breast cancer across medical images using subject-specific biomechanical models. *Medical Image Computing and Computer Assisted Intervention*, Part I, LNCS 4791:651–658, 2007.

[45] V. Rajagopal, A. Lee, J. H. Chung, and et al. Creating individual-specific biomechanical models of the breast for medical image analysis. *Academic Radiology*, 15:1425–1436, 2008.

[46] N. Ruiter, T. Muller, R. Stotzka, and et al. Automatic image matching for breast cancer diagnostics by a 3-D deformation of the mamma. *Biomedizinische Technik*, 47:644–647, 2002.

[47] N. Ruiter, R. Stotzka, T. Muller, and et al. Model-based registration of X-ray mammograms and MR images of the female breast. *IEEE transactions on nuclear science*, 53:204–211, 2006.

[48] A. Samani, J. Bishop, C. Luginbuhl, and et al. Measuring the elastic modulus of ex vivo small tissue samples. *Physics in Medicine and Biology*, 48:2183–2198, 2003.

[49] A. Samani, J. Bishop, M. J. Yaffe, and et al. Biomechanical 3-D finite element modelling of the human breast using MRI data. *IEEE Transactions on Medical Imaging*, 20:271–279, 2001.

[50] A. Samani and D. Plewes. A method to measure the hyperelastic parameters of ex vivo breast tissue samples. *Physics in Medicine and Biology*, 49:4395–4405, 2004.

[51] A. Samani, J. Zubovits, and D. Plewes. Elastic moduli of normal and pathological human breast tissues: an inversion-technique-based investigation of 169 samples. *Physics in Medicine and Biology*, 52:1565–1576, 2007.

[52] J. A. Schnabel, C. Tanner, A. D. Castellano-Smith, and et al. Validation of nonrigid image registration using finite-element methods: application to breast MR images. *IEEE Transactions on Medical Imaging*, 22:238–247, 2003.

[53] B. Seyfi, N. Fatouraee, and A. Samani. A novel micro-to-macro structural approach for mechanical characterization of adipose tissue extracellular matrix. *Journal of the Mechanical Behaviour of Biomedical Materials*, 77:140–147, 2018.

[54] P. A. Shoemaker, D. Scheider, M. C. Lee, and Y. C. Fung. A constitutive model for two-dimensional soft tissues and its application to experimental data. *Journal of Biomechanics*, 19 (6):695–702, 1986.

[55] A. M. Sims, T. Stait-Gardner, L. Fong, and et al. Elastic and viscoelastic properties of porcine subdermal fat using MRI and inverse FEA. *Biomechanics and Modeling in Mechanobiology*, 9:703–711, 2010.

[56] G. Sommer, M. Eder, L. Kovacs, and et al. Multiaxial mechanical properties and constitutive modeling of human adipose tissue: a basis for preoperative simulations in plastic and reconstructive surgery. *Acta Biomaterialia*, 9 (11):9036–9048, 2013.

[57] C. Then, T. J. Vogl, and G. Silber. Method for characterizing viscoelasticity of human gluteal tissue. *Journal of Biomechanics*, 45:1252–1258, 2012.

[58] K. L. Troyer, D. J. Estep, and C. M. Puttlitz. Viscoelastic effects during loading play an integral role in soft tissue mechanics. *Acta Biomaterialia*, 8:234–243, 2012.

[59] S. L-Y. Woo, B.R. Simon, S. C. Kuej, and et al. Quasi-linear viscoelastic properties of normal cartilage. *Journal of Biomechanical Engineering*, 102:85–90, 1980.

[60] M. Zain-Ul-Abdein, F. Morestin, L. Bouten, and et al. Numerical simulation of breast deformation under static conditions. *Computer Methods in Biomechanics and Biomedical Enginnering*, 16(S1):50–51, 2013.

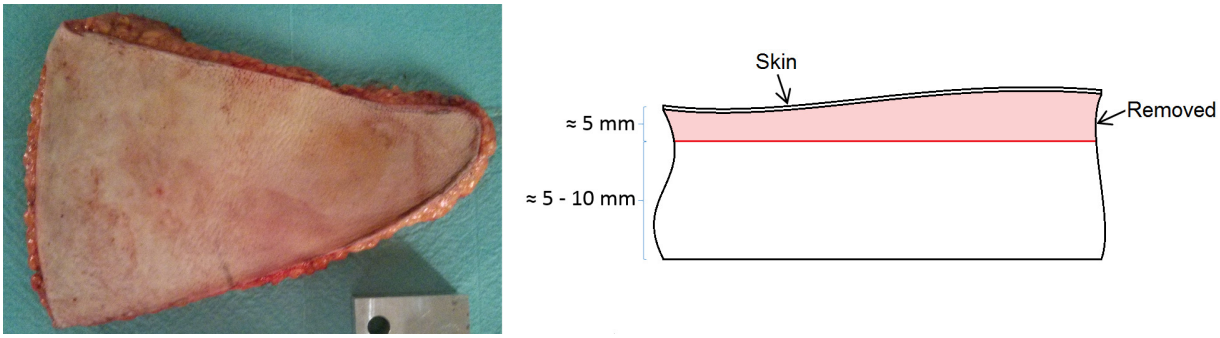

Figure 1: Piece of abdominal adipose tissue from which the specimens were extracted. The most superficial layer (in light red) was removed to obtain a sample with parallel faces.

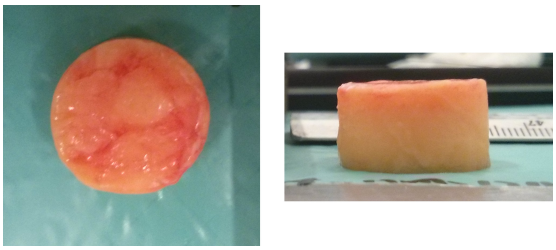

Figure 2: Cylindrical specimen, top and lateral view.

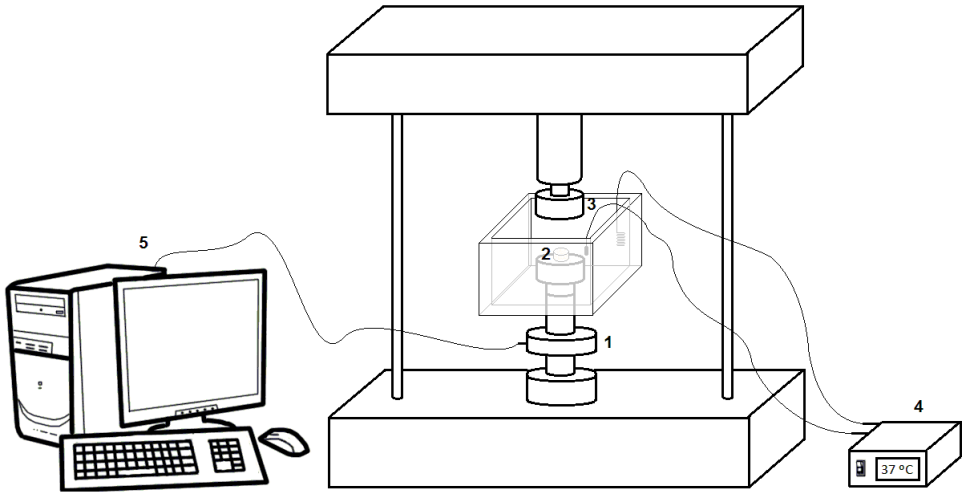

Figure 3: Scheme of the experimental setup: (1) loading cell, (2) sample, (3) upper platen, (4) temperature controller, (5) acquisition system.

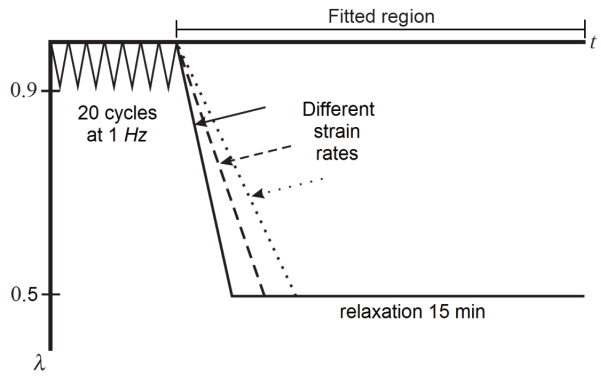

Figure 4: Scheme of the evolution of the stretch with time in the relaxation test.

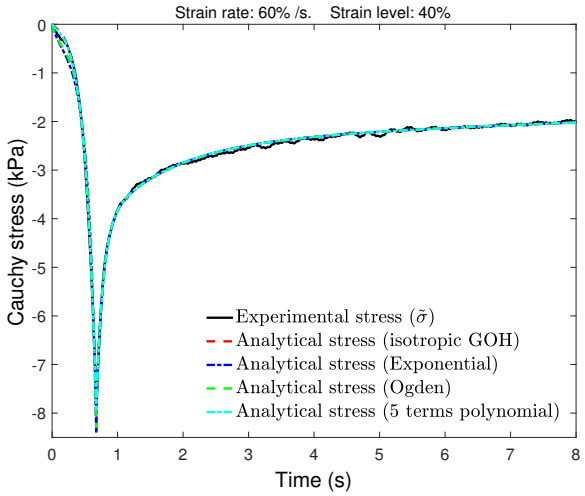

Figure 5: Example of an experimental stress record fitted with the QLV model and different SED functions for the elastic response.

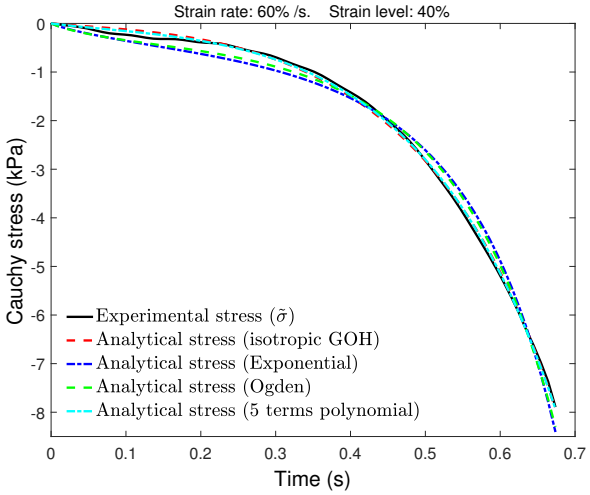

Figure 6: Detail of figure 5 corresponding to the the loading ramp.

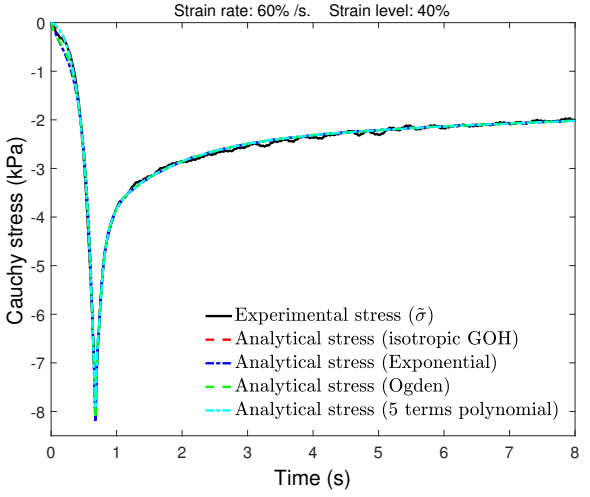

Figure 7: Example of an experimental stress record fitted with the IVV model and different SED functions for the elastic response.

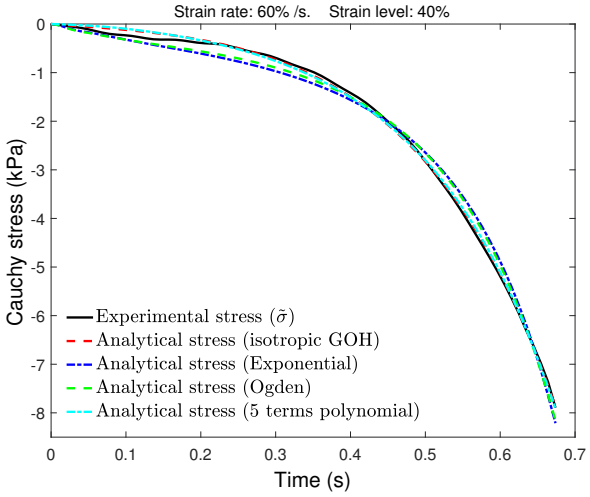

Figure 8: Detail of figure 7 corresponding to the the loading ramp.